Journal of Catalysis 280 (2011) 60–67

Contents lists available at ScienceDirect

Journal of Catalysis

journal homepage: www.elsevier.com/locate/jcat

Complete elimination of indoor formaldehyde over supported Pt catalysts with extremely low Pt content at ambient temperature

Haibao Huang *, Dennis Y.C. Leung *

Department of Mechanical Engineering, The University of Hong Kong, Pokfulam Road, Hong Kong

ARTICLE INFO

Article history:
Received 3 November 2010
Revised 28 February 2011
Accepted 4 March 2011
Available online 3 April 2011

Keywords:
Catalytic oxidation
Pt nanoparticles
Metallic Pt
HCHO elimination
Ambient temperature

ABSTRACT

A series of highly active supported Pt catalysts, developed by sodium borohydride reduction under mild preparation conditions, were used to eliminate indoor formaldehyde (HCHO) at ambient temperature. The influences of oxidation state, support and size of Pt particles, and the operating parameters were investigated. The reduced Pt nanoparticles with different supports are highly active for catalytic oxidation of HCHO. For example, nearly 100% HCHO conversion was obtained on the reduced Pt/TiO_2 catalysts (denoted as $Pt–TiO_2$) even with 0.1% Pt loading while it was less than 25% on the oxidized ones. Negatively charged metallic Pt nanoparticles, which probably facilitate the electron transfer and formation of active oxygen, provide the active sites for HCHO oxidation. The turnover frequencies (TOFs) of HCHO oxidation on Pt nanoparticles with different supports are not sensitive to the reducibility of support but somewhat affected by the Pt particle sizes. A maximum TOF of 2.87 s^{-1} was obtained on the 1% Pt–MgO with Pt particle size of about 3 nm. The 0.1% $Pt–TiO_2$ catalyst remained highly active and stable in humid air with a wide gas hourly space velocity range between 40,000 and 240,000 h^{-1} and initial HCHO concentration range between 5 and 30 ppm.

1. Introduction

Formaldehyde (HCHO), commonly emitted from construction and decorative materials for buildings, is one of the major indoor air pollutants [1–5]. Long-term exposure to indoor air containing HCHO, even a few ppm, may cause adverse effects on human health [6,7]. Great efforts have been made to reduce the indoor HCHO concentration to satisfy the stringent environmental regulations. Conventional physical adsorption and/or chemical reaction with impregnated potassium permanganate and organic amine were efficient for HCHO elimination, but these adsorbents were effective for a short period only due to their limited removal capacities [8–10]. Catalytic oxidation is recognized as the most promising HCHO removal technology [10–13], which, however, can only occur at high temperature [6,14,15] or illumination by light sources [16–18] over most of the reported catalysts. For example, 100% HCHO conversion was achieved at 453 K over a $MnO_x–SnO_2$ catalyst [15] and a maximum HCHO conversion (64.0%) was obtained over a N,S-codoped TiO_2 photocatalyst with visible light irradiation [18]. In these cases, an extra heating or illumination apparatus is needed, causing higher operating cost and more severe reaction conditions. Therefore, it is not suitable for the control of indoor air pollution [6]. Catalytic oxidation of HCHO at room temperature is highly desirable due to its environmental-friendly reaction conditions and energy-saving consideration [10,11,19]. For indoor air cleaning, low energy demand and low concentration of HCHO strongly require a catalyst to exhibit high activity for complete oxidation of HCHO. However, the development of effective catalysts for the complete oxidation of low-concentration HCHO at ambient temperature is still a challenging subject for scientists [8,10].

Recently, several studies have been carried out on removing HCHO at low temperature and even at ambient temperature using supported noble metal catalysts [2,10,11,14,20,21]. For example, 0.73% gold/iron-oxide catalysts (mass concentration, hereinafter inclusive) showed no activity in HCHO oxidation at room temperature; however, complete HCHO oxidation was obtained at 80 °C when the gold content was increased to 7.1% [14]. Álvarez-Galván et al. [22] reported that 100% HCHO conversion was achieved over a Pd/Al_2O_3 catalyst at 363 K. Particularly, Pt/TiO_2 is found most active for HCHO oxidation among the supported noble catalysts [11,20]. Zhang and He [20] reported that HCHO could be completely oxidized into CO_2 and H_2O over 1 wt% Pt/TiO_2 at room temperature. Peng and Wang [9] found that HCHO conversion was only 14.3% at 20 °C and increased to 97% at 120 °C on the 1% Pt/TiO_2 catalyst. Although supported Pt catalysts have been proved to be effective for HCHO oxidation at low temperature, even at room temperature in some cases, however, high loading of Pt is generally

* Corresponding authors. Fax: +852 2858 5415.
E-mail addresses: seabao8@gmail.com (H. Huang), ycleung@hku.hk (D.Y.C. Leung).

0021-9517/$ - see front matter © 2011 Elsevier Inc. All rights reserved.
doi:10.1016/j.jcat.2011.03.003

needed for effective oxidation of HCHO, which greatly limits its widespread application due to the expensive cost of Pt [6]. One alternative is to use cheap transition metal oxides, such as Co_3O_4, MnOx, and CeO_2, to substitute noble metal [6,7,23]. However, low efficiencies of these catalysts at room temperature limited their application [20]. Another alternative is to improve the catalytic activity and lower the Pt loading in Pt/TiO_2. In addition, the Pt catalysts for HCHO oxidation are generally pretreated in air at high temperature [8,10,11,20], which results in much energy consumption and the formation of PtOx. As known, Pt oxidation state is one of the most important factors controlling the catalytic activity [24]. The effect of metallic Pt on catalytic activity and the mechanism leading to high activity for HCHO oxidation at room temperature has not well demonstrated yet.

Herein, a series of highly efficient supported Pt catalysts were developed by sodium borohydride ($NaBH_4$) reduction under mild preparation conditions. Hydrogen is readily generated by $NaBH_4$ hydrolysis in H_2PtCl_6 solution, and Pt^{4+} can be easily reduced into metallic state by hydrogen at ambient temperature. The supported Pt catalysts were used to catalytically oxidize indoor HCHO at room temperature. The support and size of Pt particles and the operating parameters were investigated. The influence of Pt oxidation state and particle sizes, supports (i.e., TiO_2, Al_2O_3, CeO_2, ZrO_2, and MgO), and operating parameters (i.e., relative humidity, initial toluene concentration, and gas hourly space velocity (GHSV)) on catalytic activity was studied. Structural analysis of the catalysts were performed and subsequently correlated with their catalytic performances to investigate the mechanism leading to the high activity. The reduced catalysts, even with 0.1 wt% Pt loading, possess very high catalytic activity and excellent stability for HCHO oxidation at room temperature without any energy consumption. These catalysts have the advantage in low cost of preparation and use, which makes them possible to be widely applied in indoor HCHO purification.

2. Experimental

2.1. Catalyst preparation

Both oxidized and reduced Pt/TiO_2 catalysts were prepared using TiO_2 powder (P25, Degussa) as the support and H_2PtCl_6 as the Pt precursor compound. The oxidized Pt/TiO_2 catalysts (denoted as $PtO–TiO_2$) with 0.1% and 1% Pt loading were prepared via impregnation. Briefly, TiO_2 support was added into the H_2PtCl_6 solution under stirring. After impregnation for 1 h, the suspension was dried at 80 °C under stirring. The dried samples were heated at 120 °C for 4 h, followed by the calcinations at 400 °C in air for 4 h. The reduced Pt/TiO_2 catalysts (denoted as $Pt–TiO_2$) with 0.1% and 1% Pt loading were prepared by $NaBH_4$ reduction. Briefly, TiO_2 support was uniformly dispersed into the H_2PtCl_6 solution. After impregnation for 1 h, $NaBH_4$ solution was quickly added into the suspension under vigorous stirring. After reduction, the suspension was dried at 80 °C under stirring. Finally, the samples were dried at 120 °C in air for 4 h without further calcination at high temperature. Al_2O_3, CeO_2, ZrO_2, and MgO (all from Wan Jing Co. Ltd.) supported 1% reduced Pt catalysts were also prepared by $NaBH_4$ reduction with the same procedures as the 1% $Pt–TiO_2$, referring to $Pt–Al_2O_3$, $Pt–CeO_2$, $Pt–ZrO_2$, and Pt–MgO, respectively.

2.2. Catalyst characterization

Transmission electron microscopy (TEM) images were recorded on a Tecnai G2 20 microscope operated at 200 kV. X-ray powder diffraction (XRD) patterns were collected with a Bruker D8 Advance X-ray powder diffractometer operated at 40 kV and 100 mA, using Cu Kα (λ = 1.5418 Å) radiation. The intensity data were collected in a 2θ range from 20° to 90°. BET surface areas of the samples were measured by N_2 adsorption–desorption isotherms at 77 K using a Micromeritics ASAP 2020 instrument. Prior to the measurement, the samples were degassed at 523 K for 2 h. X-ray photoelectron spectroscopy (XPS) measurements of the catalysts were performed with a Physical Electronics 5600 multitechnique system using a monochromatic Al Kα source for the surface composition. The binding energy (BE) was determined by utilizing C1s line as a reference with energy of 285.0 eV. The Pt dispersion was determined by pulse CO chemisorption on a Micrometrics AutoChem II 2920 instrument at room temperature, using a thermal conductivity detector (TCD) to monitor CO consumption. A CO/Pt average stoichiometry of 1 has been assumed for the calculation of dispersion [25,26]. Prior to chemisorption, the catalyst was reduced in a stream of 10% H_2 diluted with helium at 200 °C for 60 min to remove its surface oxygen and then followed by cooling down to room temperature in a helium stream.

2.3. Measurement of catalytic activity

The catalytic oxidation of HCHO was performed in a quartz tubular (i.d. = 6 mm) fixed-bed reactor under atmospheric pressure at ambient temperature (25 ± 1 °C). Then, 0.5 g of the catalyst in 40–60 mesh was loaded in the reactor. An air mixture, containing 10 ppm HCHO and water vapor (50% relative humidity), was introduced as the reactants. Gaseous HCHO was generated by passing a stream of zero air through an HCHO solution in an incubator. The total flow rate was 1 L/min, corresponding to a GHSV of 80,000 h^{-1}. The HCHO and CO_2 in the airstream were analyzed by an HCHO monitor (Formaldemeter 400, PPM Technology) and a CO_2 monitor (HAL-HCO201, Chinaway Environment Instrument). Noted that it is difficult to make a direct comparison of the kinetic behavior of different Pt catalysts since they have different particle sizes and Pt loading and different numbers of Pt surface atoms. Apart from HCHO removal efficiency, the turnover frequency (TOF) (i.e., number of molecules reacted per Pt surface atom) is also used to evaluate the catalytic activities since it allows a better comparison of the rates for different Pt loadings, particle sizes, and supports.

3. Results and discussion

3.1. Catalyst characterization

3.1.1. TEM

Representative TEM micrographs of the supported Pt catalysts are presented in Fig. 1, and their Pt particle sizes estimated from TEM are listed in Tables 1 and 2. It can be found that small and homogeneous Pt nanoparticles (Fig. 1b and d) are uniformly present on the $Pt–TiO_2$ catalysts, whereas no distinguishable Pt particles are observed over the $PtO–TiO_2$ catalyst (Fig. 1a and c), which is consistent with the observation in the previous study [11]. Different preparation methods lead to different size and morphology of Pt particles. Reduction treatment probably promotes the formation of Pt clusters. It also can be observed that density of Pt nanoparticles over the 1% $Pt–TiO_2$ catalyst is larger than that over the 0.1% $Pt–TiO_2$ catalyst, which is consistent with their Pt loading. However, the mean size of Pt nanoparticles over the 0.1% $Pt–TiO_2$ catalyst is only about 1.8 nm, which is greatly decreased compared with that of about 2.5 nm over the 1% $Pt–TiO_2$ catalyst. High Pt concentration leads to the aggregation and growth of Pt clusters during the preparation. In addition, the reduced Pt particles with different metal oxide supports also show varied size and morphology. The Pt particle sizes estimated from TEM images range from 2.4 nm to 5.2 nm

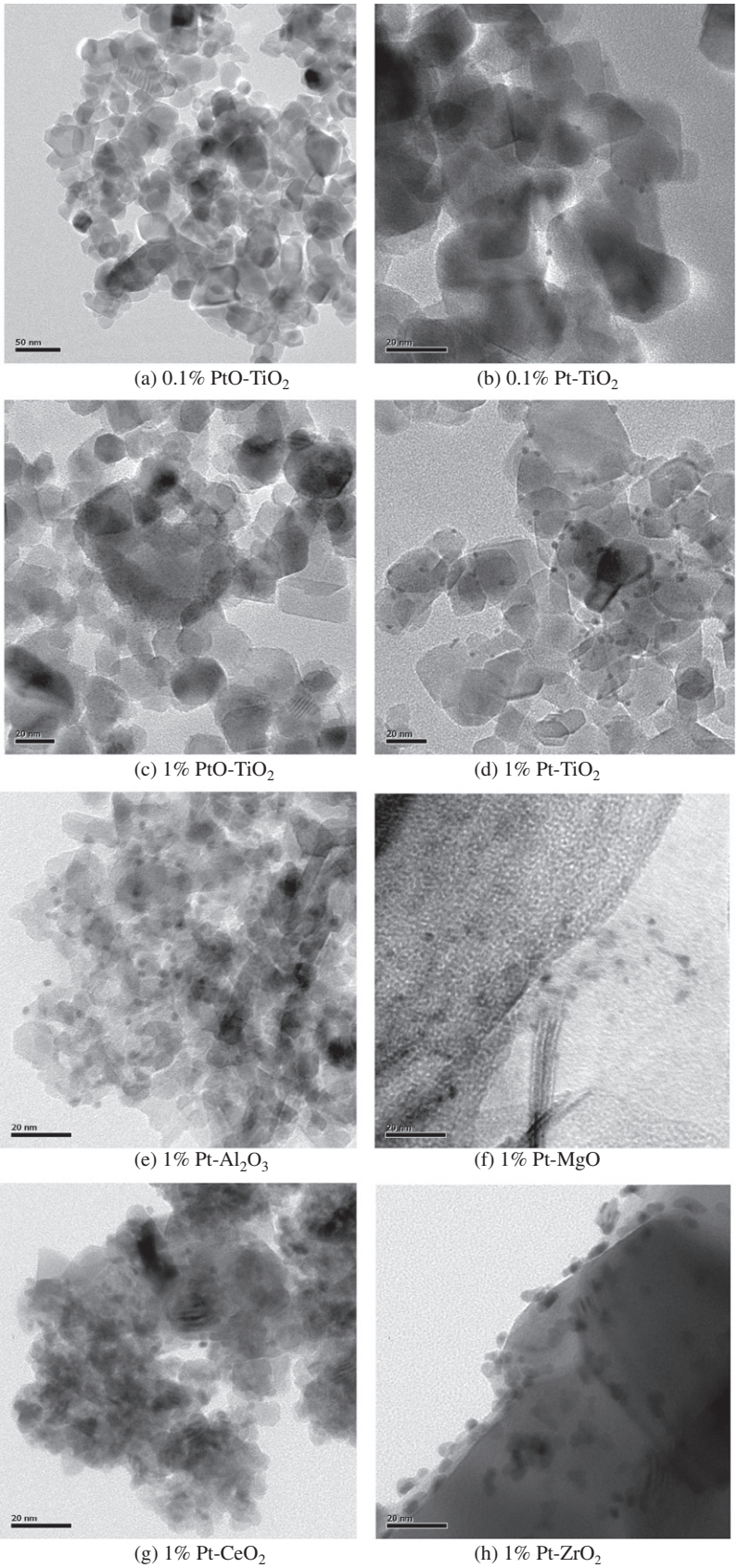

(a) 0.1% PtO-TiO_2 (b) 0.1% Pt-TiO_2

(c) 1% PtO-TiO_2 (d) 1% Pt-TiO_2

(e) 1% Pt-Al_2O_3 (f) 1% Pt-MgO

(g) 1% Pt-CeO_2 (h) 1% Pt-ZrO_2

Fig. 1. TEM images of the supported Pt catalysts.

(see Table 2). They are dispersedly distributed on the 1% Pt–TiO_2 and 1% Pt–Al_2O_3 but somewhat aggregated on the 1% Pt–ZrO_2. $NaBH_4$ reduction is a simple and mild method for the preparation of small supported Pt nanoparticles.

Table 1
BET surface areas, BE of Pt $4f_{7/2}$, Pt dispersion and particle sizes, and the TOFs of HCHO oxidation on the reduced and oxidized Pt/TiO_2 catalysts together with pure TiO_2.

Sample	BET surface area (m^2/g)	BE of Pt $f_{7/2}$ (eV)	d_{TEM} (nm)[a]	d_{CO} (nm)[b]	Pt dispersion (%)	TOF (s^{-1})[c]
TiO_2	50.8	–	–	–	–	–
0.1% PtO–TiO_2	50.9	72.4	–	4.03	27.35	0.05
1% PtO–TiO_2	52.3	72.4	–	7.59	14.83	0.05
0.1% Pt–TiO_2	51.9	70.2	1.8	2.77	41.91	2.01
1% Pt–TiO_2	43.2	70.2	2.5	3.96	28.62	2.12

[a] Average Pt particle size estimated from TEM images, hereinafter inclusive;
[b] Average Pt particle size calculated by CO chemisorptions assuming that the metal particle to be hemisphere, hereinafter inclusive;
[c] The TOF is calculated on the basis of surface Pt atoms per second, and the conversion of HCHO is kept below 60% by adjusting GHSV, hereinafter inclusive.

Table 2
BET surface areas, Pt dispersion and particle sizes, and the TOFs of HCHO oxidation on the Pt catalysts with different supports.

Sample	BET surface area (m^2/g)	d_{TEM} (nm)	d_{CO} (nm)	Pt dispersion (%)	TOF (s^{-1})
1% Pt–Al_2O_3	140.1	2.4	3.80	29.79	1.92
1% Pt–TiO_2	43.2	2.5	3.96	28.62	2.12
1% Pt–MgO	59.0	3.0	8.10	13.98	2.87
1% Pt–CeO_2	22.6	3.3	10.81	10.47	2.56
1% Pt–ZrO_2	1.43	5.2	12.92	8.79	1.05

3.1.2. XRD

The crystal structure of the Pt/TiO_2 catalysts together with pure TiO_2 was revealed by XRD, as shown in Fig. 2. The XRD patterns of both reduced and oxidized Pt/TiO_2 catalysts are essentially the same as that of pure TiO_2, which mainly exists in anatase and rutile crystal phase. No sharp peaks for Pt can be observed in them, indicating that Pt nanoparticles are well uniformly dispersed and their crystal size are very small [9,11,14], as observed in the TEM images (Fig. 1).

3.1.3. BET surface areas

The BET surface areas of Pt/TiO_2 catalysts together with pure TiO_2 are listed in Table 1. The surface areas of the Pt/TiO_2 catalysts kept almost the same as pure TiO_2 except the 1% Pt–TiO_2 catalyst. Ultrafine Pt particles are uniformly dispersed over the PtO–TiO_2, which impose little effect on the surface area. However, Pt nanoparticles on the Pt–TiO_2 would cover the surface of TiO_2 and block its pores, resulting in the decrease in surface area. More importantly, $NaBH_4$ used for Pt reduction can affect and change the surface area of TiO_2 since the deposition–precipitation is concurrent during the reduction treatment. NaOH was formed as $NaBH_4$ was added into the suspension, resulting in the increase in pH value. For example, the pH value reached 9.4 after reduction during the preparation of the 1% Pt–TiO_2. Since the Pt nanoparticles are very small, and the Pt content and the dose of reducing agent are very low on the 0.1% Pt–TiO_2 catalyst, its surface area kept almost the same as the pure TiO_2. BET surface areas of the 1% Pt–Al_2O_3, 1% Pt–MgO, 1% Pt–TiO_2, 1% Pt–CeO_2, and 1% Pt–ZrO_2 are 140.1, 59.0, 43.2, 22.6, and 1.43 m^2/g, respectively, as shown in Table 2. They impose much effect on the size and dispersion of Pt particles. It can be found that the Pt catalysts with higher BET surface areas generally obtained smaller Pt particles except the 1% Pt–TiO_2. It is reasonable that the metal particles are farther apart on a higher surface area support, such that they can maintain their small sizes better [27].

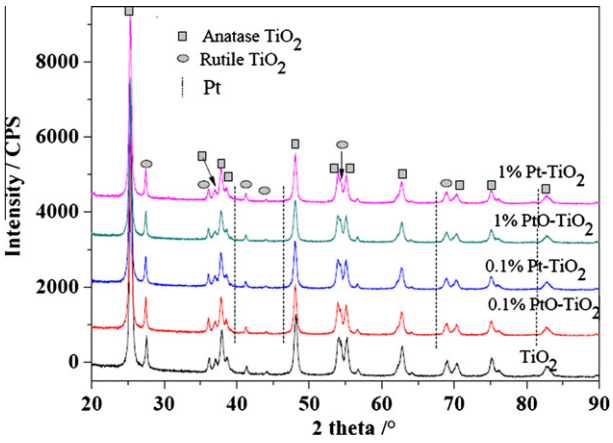

Fig. 2. XRD patterns of TiO_2 and the Pt/TiO_2 catalysts.

3.1.4. XPS

The XPS analysis was carried out to identify the surface oxidation states of the Pt particles, as shown in Fig. 3. XPS peaks for Pt 4f of the 0.1% Pt–TiO_2 and 0.1% PtO–TiO_2 catalyst are not significant due to the low Pt content. It is known that the Pt $4f_{7/2}$ BE of Pt^0, Pt^{2+}, and Pt^{4+} are around 71.1, 72.4, and 74.2 eV, respectively [28]. The peak of Pt $4f_{7/2}$ is centered at 72.4 eV on the PtO–TiO_2 catalysts, corresponding to Pt^{2+}. However, it is negatively shifted to 70.2 eV on the Pt–TiO_2 catalysts, which is far from the BE of Pt^{2+} and Pt^{4+} but close to the BE of Pt^0, indicating that Pt nanoparticles on them are fully reduced into metallic state. The main peaks of O 1s and Ti $2p_{3/2}$ on the PtO–TiO_2 catalysts are located at 530.3 and 459.0 eV, respectively, which are close to the lattice oxygen and Ti^{4+} of TiO_2 [29]. In comparison, they make a significant negative shift of 0.6 and 0.5 eV on the Pt–TiO_2 catalysts.

3.1.5. Pt dispersion

The Pt dispersion and particle size determined by pulse CO chemisorption are listed in Tables 1 and 2. It can be observed that the Pt dispersion is 41.91% on the 0.1% Pt–TiO_2 and 27.35% on the 0.1% PtO–TiO_2, which is much larger than that of 28.62% and 14.83% on the corresponding oxidized ones. As described previously, deposition–precipitation was concurrent during the reduction treatment, which resulted in a better Pt dispersion compared with the impregnation method [30]. A similar phenomenon is observed on the Pd/CeO_2 catalysts prepared by deposition–precipitation and impregnation methods [31]. Compared with the Pt/TiO_2 catalysts, the Pt/TiO_2 catalysts obtain higher Pt dispersion. The result is in agreement with the observation in TEM images that the 0.1% Pt–TiO_2 with higher Pt dispersion possesses smaller Pt particle size compared with the 1% Pt–TiO_2. It is easier to get a better Pt dispersion on TiO_2 supports with lower Pt loading. The Pt dispersion and particle size also greatly differ on different supports. Their Pt dispersion is decreased in the following order: 1% Pt–Al_2O_3 > 1% Pt–TiO_2 > 1% Pt–MgO > 1% Pt–CeO_2 > 1% Pt–ZrO_2, while the Pt

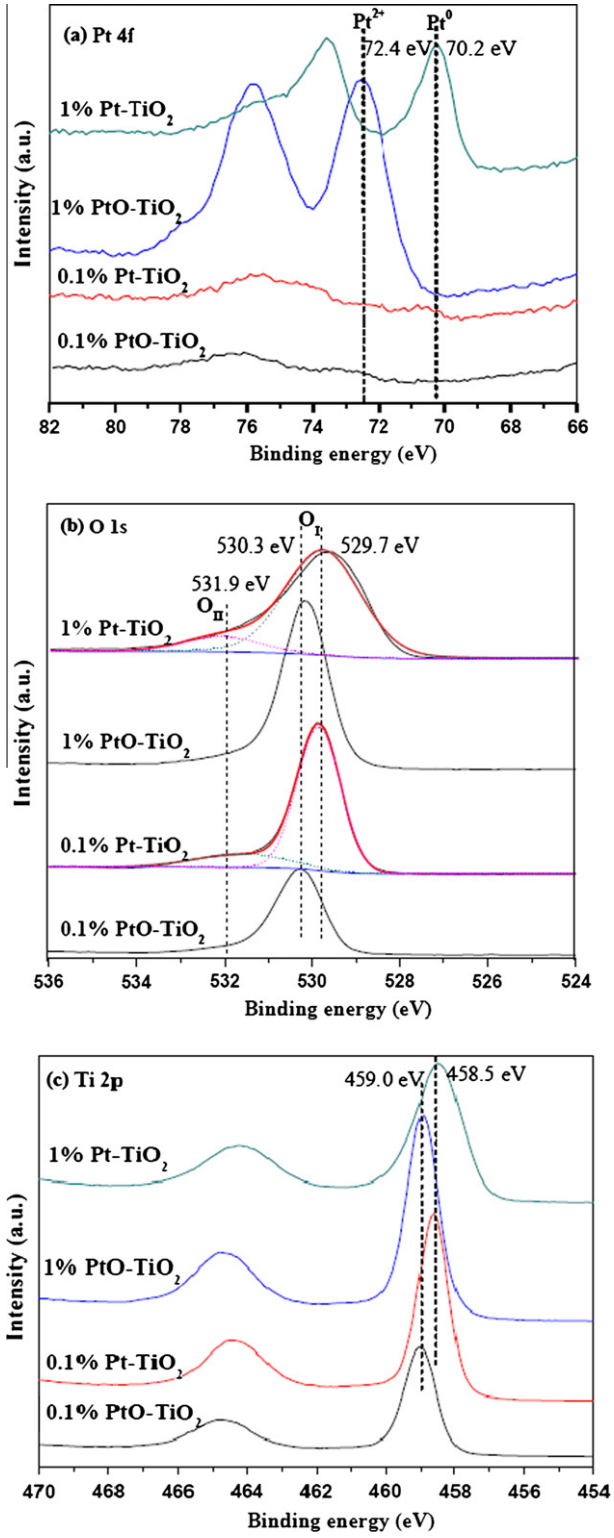

Fig. 3. XPS spectra of the PtO–TiO_2 and Pt–TiO_2 catalysts: Pt 4f (a), O 1s (b), and Ti 2p (c).

particle sizes follow the reverse order. They are closely related to the BET surface areas. The Pt catalysts with higher BET surface of supports achieved better Pt dispersion probably due to more loading sites for Pt particles. Compared to the 1% Pt–MgO, the 1% Pt–TiO_2 possessed lower BET surface area but better Pt dispersion probably due to its strong metal–support interaction (SMSI). The Pt dispersion from CO chemisorption on different supports well agrees with the observation of TEM images in Fig. 1 where the Pt particles on the 1% Pt–Al_2O_3 and 1% Pt–TiO_2 show the superior distribution while the dispersion is the lowest on the 1% Pt–ZrO_2. These particle sizes, according to TEM images, are somewhat smaller than that derived from CO chemisorption. The discrepancy could have to do with the assumptions regarding CO adsorption stoichiometry and particle morphology made in the interpretation of the CO adsorption data. With TEM, only a limited number of specimens can be examined [32].

3.2. Activity measurement

Fig. 4 compares HCHO removal efficiency of the reduced and oxidized Pt/TiO_2 catalysts at ambient temperature. HCHO oxidation by pure TiO_2 can be excluded since no CO_2 was identified during the reaction. The removal of HCHO at initial stage over pure TiO_2 and 0.1% and 1% PtO–TiO_2 is mainly ascribed to the adsorption by the TiO_2 support. Only 4.5% and 25.4% HCHO conversion was obtained at the stable stage over the 0.1% and 1% PtO–TiO_2 catalyst, respectively. However, it was remarkably increased to 99.1% and 98.8% over the 0.1% and 1% Pt–TiO_2 catalyst, respectively. Note that the Pt loading of the 0.1% Pt–TiO_2 catalyst was only 1/10 of the 1% Pt–TiO_2 catalyst while almost the same high magnitude of HCHO conversion as the latter was obtained. Their activity data were normalized on the basis of surface Pt atom from CO chemisorptions and compared in terms of TOF. As shown in Table 1, the TOF of HCHO oxidation is 2.01 s^{-1} on the 0.1% Pt–TiO_2, which is close to 2.12 s^{-1} on the 1% Pt–TiO_2, indicating that the specific activities of the Pt–TiO_2 catalysts do not much depend on Pt loading in this study. The high HCHO removal efficiency on the 0.1% Pt–TiO_2 was probably due to the high TOF of HCHO oxidation on metallic Pt nanoparticles and its high BET surface area and Pt dispersion, which can provide adsorption sites and active centers for HCHO oxidation.

Catalytic activity of HCHO oxidation was significantly improved over the reduced Pt/TiO_2 catalyst when compared with the oxidized ones. Different pretreatment of Pt will result in different valence state of Pt, thus affecting the HCHO removal efficiency. The Pt–TiO_2 catalysts with metallic Pt achieved much higher HCHO conversion than the oxidized ones with cationic Pt (see Fig. 4), suggesting that metallic Pt rather than cationic Pt nanoparticles provides the active sites for HCHO oxidation. The former achieves about 40 times of TOF of HCHO oxidation than the later (see Table 1). It is worth noting that Pt $4f_{7/2}$ of the Pt–TiO_2 is negatively shifted to a lower BE by approximately 1 eV compared with bulk

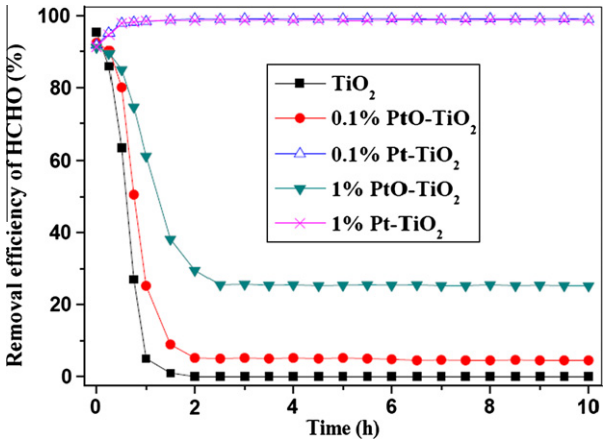

Fig. 4. Time dependence of HCHO conversion for TiO_2 and the Pt/TiO_2 catalysts at ambient temperature (HCHO concentration = 10 ppm, relative humidity = 50% and GHSV = 80,000 h^{-1}).

metallic Pt with typical Pt $4f_{7/2}$ BE around 71.2 eV, indicating an increase in the electron density on Pt particles of the Pt–TiO_2 catalysts [33]. The electrons were proposed to be transferred from TiO_2 due to a SMSI [34]. The SMSI on the Pt–TiO_2 catalyst prepared by $NaBH_4$ liquid reduction is even much more profound than that prepared by hydrogen reduction, whose Pt $4f_{7/2}$ (around 71.0 eV) is much higher than 70. 2 eV but close to that of bulk metallic Pt. The SMSI may influence the electronic and catalytic properties of the surface Pt. Significant BE shift is also observed for O 1s and Ti 2p of the Pt–TiO_2 catalysts, as shown in Fig. 3b and c, respectively. The negative shift of Ti $2p_{3/2}$ indicated that TiO_2 is partially reduced into Ti^{3+} and oxygen vacancies are generated on the Pt–TiO_2 catalyst [35,36]. When oxygen vacancies are formed at the metal–support interface of Pt/TiO_2, oxygen from the gas phase could be dissociatively adsorbed on such defect with one of the oxygen atoms filling the vacancy and the other being coordinated to the five-coordinate Ti^{4+} site as an adatom [33]. The chemisorbed oxygen can be activated on the metal–support interface, forming highly active oxygen species that are involved in the oxidation reaction. The chemisorbed oxygen was identified by XPS on the Pt–TiO_2 catalysts (Fig. 3b), in which a significant shoulder peak of O 1s was observed at 531.9 eV while such peaks were not obvious on the oxidized ones. Metallic Pt nanoparticles and oxygen vacancies can facilitate the electron transfer, adsorption, and activation of oxygen, which probably accounts for the high activity for HCHO oxidation on the Pt–TiO_2 catalysts.

The nature of supports and particle sizes of noble metal is often regarded as possible important parameters in supported noble metal catalysts [32,29,37,38]. To see the support and size effect of the Pt particles in HCHO oxidation, Pt was supported on the reducible supports (i.e., TiO_2 and CeO_2) and irreducible supports (i.e., Al_2O_3, MgO, and ZrO_2). Varied Pt particle sizes were obtained on different supports, as previously described. The TOFs on the Pt catalysts with different supports are listed in Table 2. No obvious correlation can be observed between the catalytic activities and the reducibility of support. The Pt catalysts with irreducible supports (i.e., 1% Pt–Al_2O_3 and 1% Pt–MgO) achieved similar or even higher TOFs than those with reducible supports (i.e., 1% Pt–TiO_2 and 1% Pt–CeO_2), revealing that the catalytic activities are weakly influenced by the reducibility of support in this reaction. Our finding is in good agreement with the finding in previous study [32,39,40]. Comotti et al. [39] prepared Au supported on TiO_2, Al_2O_3, ZnO, and ZrO_2 by adsorption of Au colloids onto the supports and found no correlation between the order of activity and the reducibility of the support. The Au colloids were prepared by $NaBH_4$ reduction at room temperature, which is similar to the procedure for preparing the supported Pt catalysts in this study. Okamura et al. [40] prepared catalysts with dimethylauric acetylacetonate by CVD on Al_2O_3, SiO_2, and TiO_2 and observed no appreciable differences in the TOFs in CO oxidation between the three catalysts. In both of the above-mentioned cases and this study, the preparation conditions for the supported noble metal catalysts are different from those in the literature where noble metals were generally prepared by impregnation, coprecipitation, or deposition–precipitation followed by annealing at high temperature [37,41]. The insensitivity to reducibility of support in this study is probably attributed to the mild conditions for preparing the Pt catalysts and specific reaction conditions (such as HCHO reactants and room-temperature reaction condition).

Although the activities of Pt catalysts are not sensitive to the reducibility of support, the Pt particle sizes are greatly influenced by the nature of supports (such as BET surface area and support-metal interaction). As shown in Table 2, the specific catalytic activities in terms of TOFs present somewhat size-dependent effect. The TOF of HCHO oxidation was increased from 1.92 to 2.87 s^{-1} with increasing Pt particle size ranging from 2.4 nm to 3 nm (d_{TEM}, hereinafter inclusive). A maximum TOF value was obtained on the 1% Pt–MgO with Pt particle size of about 3 nm. However, further increase in Pt particle size instead led to the drop of TOF. A minimal TOF of 1.05 s^{-1} was obtained on the 1% Pt–ZrO_2 with Pt particle size of about 5.2 nm. An optimum Au particle size of 2–4 nm was also observed during low-temperature oxidation of CO over Au catalysts with different supports [42], and the maximum TOF of methane oxidation was observed on the Al_2O_3-supported Pt catalysts with the mean particle sizes of about 2 nm [38]. As the particle size increases, the number of Pt atoms on (1 0 0) and (1 1 1) crystal facets increases with respect to those at edges and corners, and the (1 0 0) and (1 1 1) crystal facets of Pt provide appropriate sites for reaction [43]. However, the decrease in activity at larger particle sizes is to be expected, since too large particles, although possessing the appropriate crystal faces, possess too little Pt surface area [32]. The dramatic decrease in activity on the 1% Pt–ZrO_2 probably attributed to its very low BET surface area despite its large Pt particle size.

3.3. Effect of operating parameters

The influencing factors of the catalytic reaction, including relative humidity, initial toluene concentration, and air flow rate, were studied to evaluate the catalytic activity and stability on the 0.1% Pt–TiO_2 catalyst.

3.3.1. Effect of moisture

HCHO in indoor air is often enriched with water vapor, which frequently leads to severe catalytic deactivation through the strong adsorption on the active sites, especially at low temperatures [6]. It is important for catalysts to keep active and stable under humid environments. Therefore, it is of significance to investigate the effect of moisture on HCHO oxidation at ambient temperature.

Fig. 5 investigates the effect of humidity on HCHO oxidation. HCHO removal efficiency follows the order: 25% ≈ 50% > 75% > 97.5% ≫ 0% under different relative humidity. HCHO oxidation was greatly promoted by water vapor up to 50% humidity. Nearly 100% HCHO conversion was achieved at 25% and 50% humidity while it is only 45.2% at the stable stage at 0% humidity. The presence of moisture did not inhibit but enhance HCHO oxidation at room temperature. It is reported that moisture favors the activation of oxygen and the decomposition of carbonate in the process of CO oxidation by Au catalysts, thus greatly improving the catalytic activities [44,45]. In addition, water vapor can remove chloride poison by hydrolyzing the Au–Cl bond

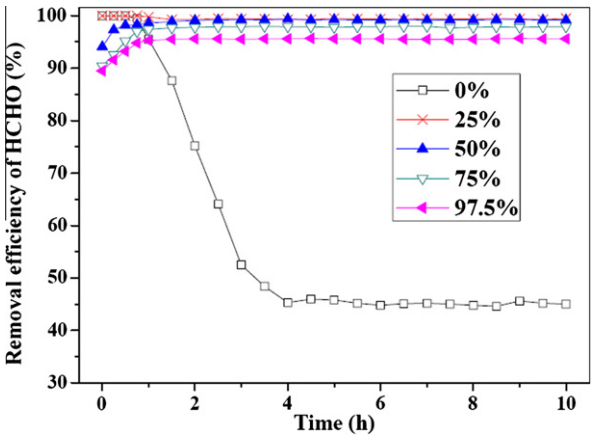

Fig. 5. Effect of relative humidity on HCHO conversion over the 0.1% Pt–TiO_2 catalyst (HCHO concentration = 10 ppm, GHSV = 80,000 h^{-1}).

and prevent the deactivation of Au catalysts [46]. Similar mechanism may exist in HCHO oxidation over Pt/TiO_2. The difference between CO and HCHO oxidation is that H_2O is a product during HCHO oxidation [21]. The Au catalyst nearly lost its activity in dry CO oxidation [45,46] while the Pt catalyst still achieved 45% HCHO conversion in dry air. The HCHO conversion was slightly dropped with the increased humidity higher than 50% due to the coverage of active centers by water [1]. However, the removal efficiency still kept as high as 95.6% at 97.5% humidity. The 0.1% Pt–TiO_2 catalyst remained highly active and stable in humid air.

3.3.2. Effect of GHSV

The effect of GHSV on HCHO conversion at room temperature was studied by fixing the initial HCHO concentration to be 10 ppm and 50% humidity. Fig. 6 compares the conversions of HCHO over the 0.1% Pt–TiO_2 catalyst at different GHSVs. The steady conversion of HCHO was 100% at 40,000 h^{-1}, 99.1% at 80,000 h^{-1}, 97.8% at 160,000 h^{-1}, and 90.5% at 240,000 h^{-1}. It decreased with increasing GHSV due to less contact time. The 0.1% Pt–TiO_2 catalyst obtained a very high HCHO conversion even at an extremely high GHSV of 240,000 h^{-1}, indicating that only a very small amount of catalyst is needed for HCHO purification. This can also greatly lower the cost of the Pt used.

3.3.3. Effect of initial concentration of HCHO

Since the indoor HCHO concentration varies in a wide range from dozens of ppb to ppm, it is worthwhile to investigate the removal of HCHO with various concentrations. The effect of initial HCHO concentration on HCHO conversion was studied by fixing 50% humidity and 80,000 h^{-1} GHSV, varying the initial HCHO concentration in the range of 5–30 ppm. As shown in Fig. 7, the steady conversion of HCHO was 100% at 5 ppm, 99.1% at 10 ppm, 98.2% at 20 ppm, and 95.8% at 30 ppm. As anticipated, HCHO removal efficiency decreased with increasing initial HCHO concentration. The 0.1% Pt–TiO_2 catalyst still exhibited very high activity for HCHO oxidation at high initial HCHO concentration. It can be anticipated that the 0.1% Pt–TiO_2 catalyst can completely eliminate indoor HCHO, whose concentration is generally lower than the experimental concentrations of HCHO.

3.3.4. Durability test

The durability of catalysts is very important to application. The durability test on the 0.1% Pt–TiO_2 catalyst was conducted by fixing 10 ppm initial HCHO concentration, 50% humidity, and 80,000 h^{-1} GHSV. As shown in Fig. 8, no significant deactivation was observed after operation for 120 h, indicating that the 0.1% Pt–TiO_2 catalyst has excellent durability.

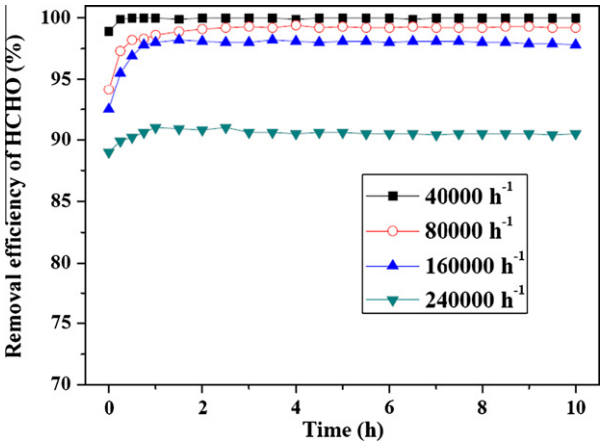

Fig. 6. Effect of GHSV on HCHO conversion over the 0.1% Pt–TiO_2 catalyst (HCHO concentration = 10 ppm, relative humidity = 50%).

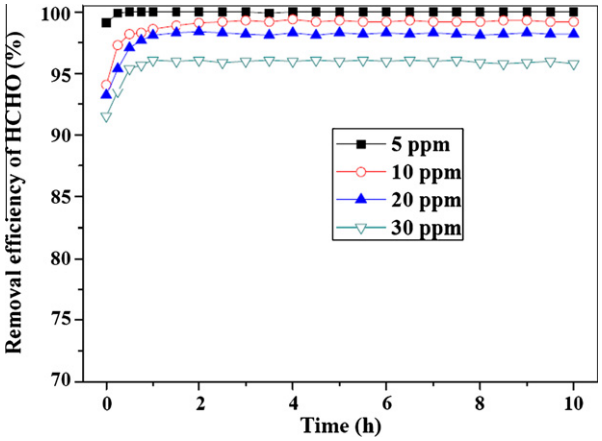

Fig. 7. Effect of initial HCHO concentration on HCHO conversion over the 0.1% Pt–TiO_2 catalyst (Relative humidity = 50%, GHSV = 80,000 h^{-1}).

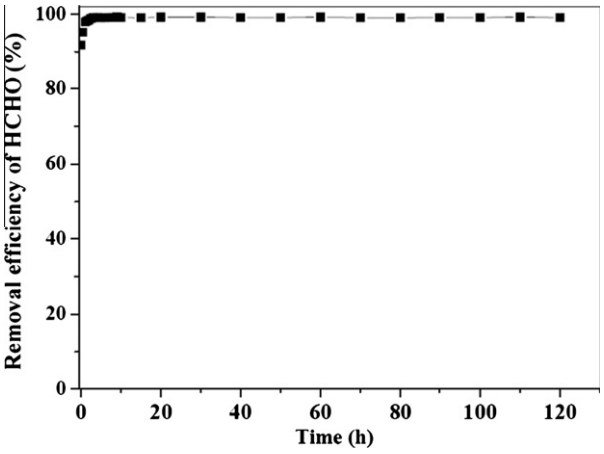

Fig. 8. Durability test on the 0.1% Pt–TiO_2 catalyst for HCHO oxidation (HCHO concentration = 10 ppm, relative humidity = 50% and GHSV = 80,000 h^{-1}).

4. Conclusions

Indoor formaldehyde from, e.g., furniture and construction materials represents a serious environmental hazard. Developing catalytic devices that degrade formaldehyde is therefore of great importance. In this paper, we have shown that TiO_2-supported Pt catalysts prepared by $NaBH_4$ reduction are highly active for catalytic oxidation of HCHO at ambient temperature. A stable formaldehyde conversion of nearly 100% can be achieved with Pt–TiO_2 systems containing only 0.1% platinum by weight. We propose that negatively charged metallic Pt nanoparticles, which probably facilitate the electron transfer and formation of active oxygen, provide the active sites for HCHO oxidation.

Acknowledgment

The authors gratefully acknowledge the financial supports from the CRCG of the University of Hong Kong (Grant No. 200907176159).

References

[1] V.A. de la Peña O'Shea, M.C. Álvarez-Galván, J.L.G. Fierro, P.L. Arias, Appl. Catal. B 57 (2005) 191.
[2] L. Wang, M. Sakurai, H. Kameyama, J. Hazard. Mater. 167 (2009) 399.
[3] T.N. Obee, R.T. Brown, Environ. Sci. Technol. 29 (1995) 1223.
[4] F. Chen, X. Yang, Q. Wu, Environ. Sci. Technol. 43 (2009) 4606.
[5] X.F. Tang, J.L. Chen, Y.G. Li, Y. Li, Y.D. Xu, W.J. Shen, Chem. Eng. J. 118 (2006) 119.
[6] X.F. Tang, Y.G. Li, X.M. Huang, Y.D. Xu, H.Q. Zhu, J.G. Wang, W.J. Shen, Appl. Catal. B 62 (2006) 265.
[7] Y. Sekine, Atmos. Environ. 36 (2002) 5543.
[8] C.B. Zhang, H. He, K. Tanaka, Catal. Commun. 6 (2005) 211.
[9] J.X. Peng, S.D. Wang, Appl. Catal. B 73 (2007) 282.
[10] X.F. Tang, J.L. Chen, X.M. Huang, Y. Xu, W.J. Shen, Appl. Catal. B 81 (2008) 115.
[11] C.B. Zhang, H. He, K. Tanaka, Appl. Catal. B 65 (2006) 37.
[12] Y.B. He, H.B. Ji, Chin. J. Catal. 31 (2010) 171.
[13] J. Peng, S. Wang, J. Phys. Chem. C 111 (2007) 9897.
[14] C. Li, Y. Shen, M. Jia, S. Sheng, M.O. Adebajo, H. Zhu, Catal. Commun. 9 (2008) 355.
[15] Y. Wen, X. Tang, J. Li, J. Hao, L. Wei, X. Tang, Catal. Commun. 10 (2009) 1157.
[16] W.H. Ching, M. Leung, D.Y.C. Leung, Sol. Energy 77 (2004) 129.
[17] T. Noguchi, A. Fujishima, P. Sawunyama, K. Hashimoto, Environ. Sci. Technol. 32 (1998) 3831.
[18] J. Yu, M. Zhou, B. Cheng, X. Zhao, J. Mol. Catal. A: Chem. 246 (2006) 176.
[19] L.F. Wang, Q. Zhang, M. Sakurai, H. Kameyama, Catal. Commun. 8 (2007) 2171.
[20] C. Zhang, H. He, Catal. Today 126 (2007) 345.
[21] Y.C. Hong, K.Q. Sun, K.H. Han, G. Liu, B.Q. Xu, Catal.Today 158 (2010) 415.
[22] M.C. Álvarez-Galván, B. Pawelec, V.A. de la Peña O'Shea, J.L.G. Fierro, P.L. Arias, Appl. Catal. B 51 (2004) 83.
[23] Y. Sekine, A. Nishimura, Atmos. Environ. 35 (2001) 2001.
[24] H. Yoshida, Y. Yazawa, T. Hattori, Catal. Today 87 (2003) 19.
[25] I. Contreras-Andrade, A. Vzquez-Zavala, T. Viveros, Energy & Fuels 23 (2009) 3835.
[26] D. Liang, J. Gao, J. Wang, P. Chen, Z. Hou, X. Zheng, Catal. Commun. 10 (2009) 1586.
[27] M.C. Kung, R.J. Davis, H.H. Kung, J. Phys. Chem. C 111 (2007) 11767.
[28] M.J. Tiernan, O.E. Finlayson, Appl. Catal. B 19 (1998) 23.
[29] X. Chen, C. Burda, J. Phys. Chem. B 108 (2004) 15446.
[30] X. Li, I.M. Hsing, Electrochim. Acta 51 (2006) 5250.
[31] L.H. Xiao, K.P. Sun, X.L. Xu, X.N. Li, Catal. Commun. 6 (2005) 796.
[32] K. Villani, W. Vermandel, K. Smets, D. Liang, G. Van Tendeloo, J. Martens, Environ. Sci. Technol. 40 (2006) 2727.
[33] O.S. Alexeev, S.Y. Chin, M.H. Engelhard, L. Ortiz-Soto, M.D. Amiridis, J. Phys. Chem. B 109 (2005) 23430.
[34] M. Aramendia, J. Colmenares, A. Marinas, J. Marinas, J. Moreno, J. Navio, F. Urbano, Catal. Today 128 (2007) 235.
[35] S. Rengaraj, X.Z. Li, J. Mol. Catal. A: Chem. 243 (2006) 60.
[36] C. Xiao-Quan, L. Huan-Bin, G. Guo-Bang, Mater. Chem. Phys. 91 (2005) 317.
[37] S. Arrii, F. Morfin, A.J. Renouprez, J.L. Rousset, J. Am. Chem. Soc. 126 (2004) 1199.
[38] I. Beck, V. Bukhtiyarov, I. Pakharukov, V. Zaikovsky, V. Kriventsov, V. Parmon, J. Catal. 268 (2009) 60.
[39] M. Comotti, W. Li, B. Spliethoff, F. Schüth, J. Am. Chem. Soc 128 (2006) 917.
[40] M. Okumura, S. Nakamura, S. Tsubota, T. Nakamura, M. Azuma, M. Haruta, Catal. Lett. 511 (1998) 53.
[41] L.F. Liotta, G. Di Carlo, G. Pantaleo, A.M. Venezia, Catal. Today 158 (2010) 56.
[42] N. Lopez, T.V.W. Janssens, B.S. Clausen, Y. Xu, M. Mavrikakis, T. Bligaard, J.K. Nørskov, J. Catal. 223 (2004) 232.
[43] M. Min, J. Cho, K. Cho, H. Kim, Electrochim. Acta 45 (2000) 4211.
[44] M. Dat, M. Haruta, J. Catal. 201 (2001) 221.
[45] M. Daté, M. umura, S. Tsubota, M. Haruta, Angew. Chem. 116 (2004) 2181.
[46] H.H. Kung, M.C. Kung, C.K. Costello, J. Catal. 216 (2003) 425.